NANO LETTERS

pubs.acs.org/NanoLett

Letter

A pH-Reversible Fluorescent Probe for *in Situ* Imaging of Extracellular Vesicles and Their Secretion from Living Cells

Hanzhuang Liu, Shaorui Liu, Yu Xiao, Wenting Song, Huize Li, Lok Wai Cola Ho, Zhen Shen, and Chung Hang Jonathan Choi*

Cite This: *Nano Lett.* 2021, 21, 9224–9232

Read Online

ACCESS | Metrics & More | Article Recommendations | Supporting Information

ABSTRACT: Our knowledge in how extracellular vesicles (EVs) are secreted from cells remains inadequate due to the limited technologies available for visualizing them *in situ*. We report a pH-reversible boron dipyrromethene (BODIPY) fluorescent probe for confocal imaging of EVs secreted from living cells without inducing severe cytotoxicity. This probe predominantly assumes a non-fluorescent leuco-BODIPY form under basic conditions, but it gradually switches to its fluorescent parent BODIPY form upon acidification; such pH transition empowers the imaging of acidic EVs (such as CD81-enriched exosomes and extracellular multivesicular bodies) in weakly basic culture medium and intracellular acidic precursor EVs in weakly basic cytoplasm, with minimal false positive signals frequently encountered for "always-on" dyes. Joint application of this probe with plasmid transfection reveals the secretion of some EVs from cellular pseudopodia *via* microtubule trackways. This probe may provide mechanistic insights into the extracellular transport of EVs and support the development of EV-based nanomedicines.

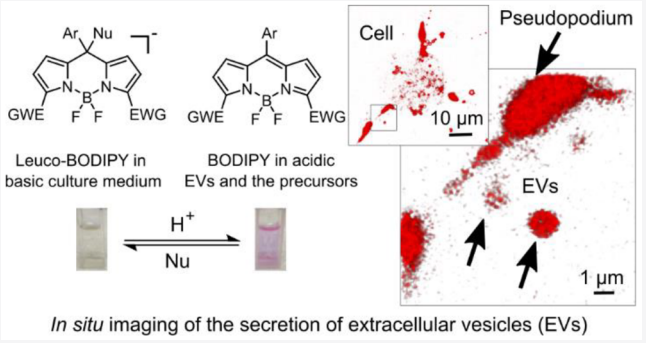

In situ imaging of the secretion of extracellular vesicles (EVs)

KEYWORDS: *fluorescent probes, exosomes, extracellular vesicles, leuco dyes, microtubules*

Extracellular vesicles (EVs), secreted by different cell types to the surrounding, mediate intercellular communication.[1,2] For example, cancer cells secrete "oncosomes" for transferring oncogenic materials to other cells.[3] EVs are also drug carriers for biomedical applications such as immunotherapy and regenerative medicine[4] due to their colloidal stability, low immunogenicity, and effective cellular entry.[5] EVs fall under two main categories, namely, ectosomes (~100−500 nm in size) formed on the cell membrane and released via outward budding and exosomes (~50−150 nm in size)[6] originating from intraluminal vesicles in the endocytic cisternae that become multivesicular bodies (MVBs) and fuse with the cell membrane for secretion.[7]

Real-time live imaging of EVs *in situ* (i.e., in cell-seeded medium without the need for harvesting the EVs in advance) will offer insights into the mechanism for secretion of EVs,[8] yet many existing imaging tools are not efficient or feasible. Transmission electron microscopy enables nanoscale visualization of EVs in general,[2] and immunofluorescence enables real-time imaging of specific types of EVs by staining markers of intracellular precursor EVs. However, both methods do not support live imaging of exocytosis because they require cell fixation. Transfecting cells with plasmids encoding EV markers fused with fluorescent reporters [e.g., green fluorescent protein (GFP)-tagged CD81, a marker for exosomes[1]] empowers confocal imaging of EV secretion from living cells *in situ*,[9,10] but this method suffers from nonuniform transfection, prolonged protein expression, and cytotoxicity that may affect exocytosis.[11,12] Fluorescent probes modified with functional groups (e.g., aliphatic and carboxylate) for binding to the EV membrane or rotor probes that fluoresce only near the EV membrane[13,14] allow for imaging of harvested EVs, but whether they support *in situ* visualization of EV secretion is unclear. Near-infrared semiconducting polyelectrolytes, when complexed with aptamers that target different exosome proteins, support the detection of different exosome types in culture medium, but it remains to be shown if they empower real-time imaging of the secretion of EVs.[15]

We report a molecular fluorescent probe for *in situ* visualization of secreted EVs in conditioned medium (i.e., medium harvested from cultured cells) and real-time secretion of extracellular MVBs, within 30 min of adding the probe to cell-seeded medium. This probe is color-shifting[16] and pH-

Received: August 12, 2021
Revised: October 28, 2021
Published: November 1, 2021

https://doi.org/10.1021/acs.nanolett.1c03110
Nano Lett. 2021, 21, 9224–9232

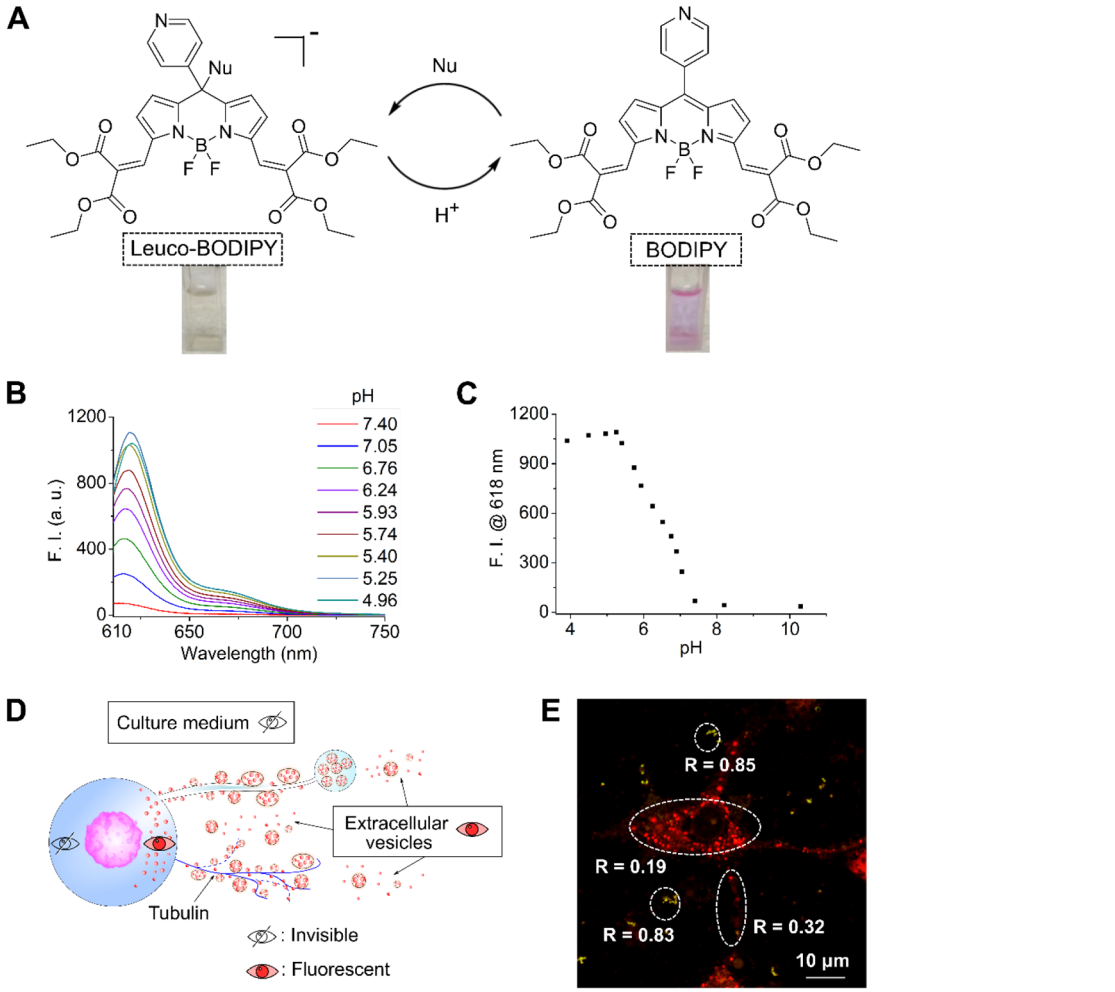

Figure 1. *In situ* detection of extracellular vesicles (EVs) in cell culture medium by the pH-reversible fluorescent probe. (A) Reversible transformation between non-fluorescent leuco-BODIPY in near-neutral culture medium (pH ~ 7.4) and fluorescent BODIPY upon acidification to pH 7. Nu: nucleophile. (B) Fluorescence emission spectrum as a function of pH in C_2H_5OH/PBS (1:1, v/v). (C) Fluorescence emission intensity at 618 nm as a function of pH. (D) Schematic illustration of *in situ* detection of EVs in conditioned medium (i.e., medium previously cultured with cells). This acid-responsive probe either directly stains EVs that are secreted by cells or enters cells to stain precursor EVs that are later secreted as EVs. Some precursor EVs exit the cell *via* microtubule trackways. (E) Representative confocal image of a HeLa cell that expresses green fluorescent protein (GFP)-tagged CD81 (marker of exosomes; green) 30 min after addition of the probe (red). Yellow color in the extracellular space indicates EVs in the medium, as evidenced by the colocalization between CD81 and BODIPY. *R* values indicate the Pearson colocalization coefficients between BODIPY and CD81-GFP.

reversible; it can transform between its non-fluorescent leuco-BODIPY form under alkaline conditions and its BODIPY form with magenta fluorescence under acidic conditions (Figure 1A). Nucleophilic attack of the central meso-carbon of the BODIPY form (say by water, hydroxide ions, thiols, or amino acids in culture medium) causes the loss of π-conjugation and >200 nm blueshift of its absorption peak to its leuco-BODIPY form; reacidification switches the leuco-BODIPY form back to the BODIPY form (Figure 1B,C). Such pH reversibility affords a "pro-fluorophore" approach[17−21] to selectively detect acidic EVs in weakly basic culture medium and intracellular acidic precursor EVs [e.g., late endosomes (pH ~ 5.5−6.0) and recycling endosomes (pH ~ 6.4−6.5)][22] in weakly basic cytoplasm with minimal background interference from free dyes,[23] obviating the need for isolating the EVs for staining and rinsing the cells to remove excess dyes before confocal imaging (Figure 1D,E). Previously, Unaleroglu et al. reported the reversible transformation between BODIPY and leuco-BODIPY forms with an onset point of fluorescence at pH ~ 10.0, but the authors did not use the dye for imaging intracellular organelles or EVs.[24] Later, we reported a pH-reversible BODIPY/leuco-BODIPY-based probe with a pK_a of 3.69 and onset point of fluorescence at pH ~ 6 for imaging the formation of acidified organelles during autophagy,[23] but we did not manage to detect extracellular fluorescence possibly because its onset point of fluorescence is more acidic than the EV lumen. Here, we adjust the onset point of fluorescence to pH ~ 7.4 to take advantage of the acidic luminal pH of EVs for detection; this strategy enables the imaging of EVs with attenuated false positive signals that are often associated with "always-on" fluorescent dyes in medium.[25,26] We demonstrate the *in situ* detection of CD81-enriched exosomes in medium seeded with three different cell types (HeLa cervix cancer cells, A549 lung cancer cells, and HEK293 embryonic kidney cells) and their respective intracellular precursor EVs without inducing severe cytotoxicity. Then, we visualize the real-time secretion of extracellular multivesicular bodies (EMVBs). Finally, we combine plasmid transfection with this probe to

https://doi.org/10.1021/acs.nanolett.1c03110
Nano Lett. 2021, 21, 9224−9232

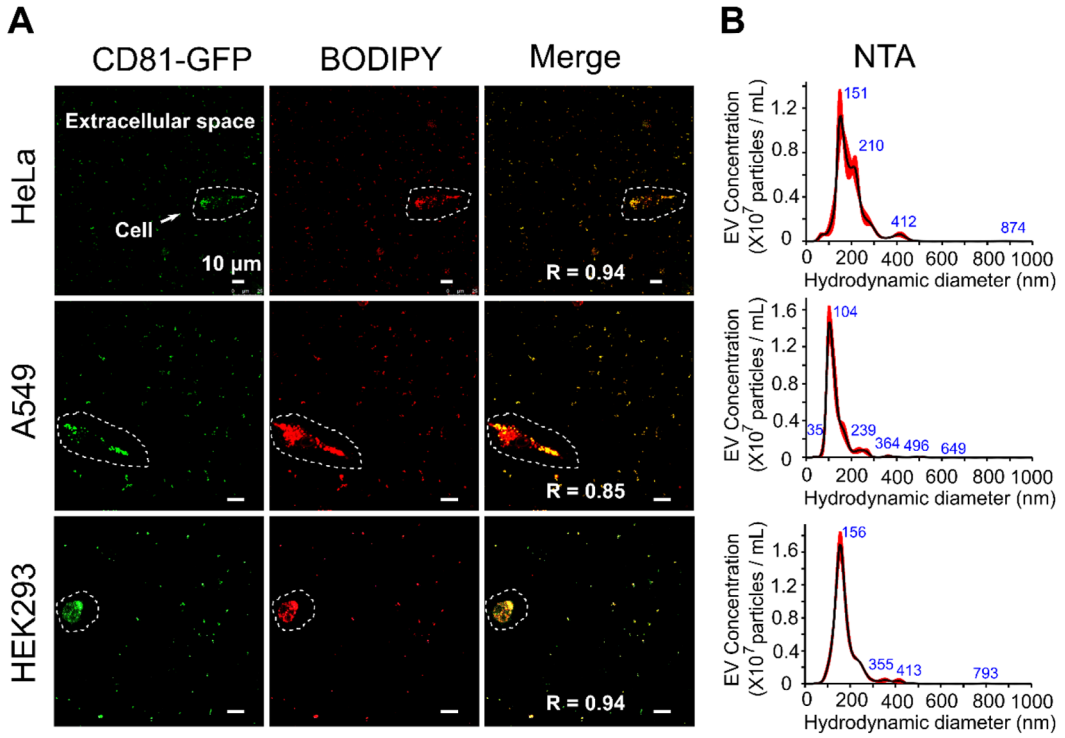

Figure 2. *In situ* detection of EVs secreted by cells to the culture medium by this probe. (A) Confocal images of HeLa cells, A549 cells, and HEK293 cells that express GFP-tagged CD81 were stained with this probe for 30 min. Note that the cells were not rinsed with PBS to retain the secreted EVs in the conditioned medium for *in situ* imaging. Scale bar = 10 μm. *R* values indicate the Pearson colocalization coefficients between the fluorescence of BODIPY (red) and CD81-GFP (green) in the extracellular region. (B) Hydrodynamic diameter distribution of the EVs secreted by the three cell types that were cultured for 24 h by nanoparticle tracking analysis (NTA).

prove the secretion of some EVs along cellular pseudopodia *via* microtubule trackways.

We prepared BODIPY by a classical method (Figures S1 and S2)[27,28] and verified its structure by high resolution mass spectrometry (HRMS; Figure S3), ^{1}H nuclear magnetic resonance (^{1}H NMR; Figure S5), and ^{13}C NMR (Figure S6). Next, we added methanol as a representative nucleophile to convert BODIPY to leuco-BODIPY; addition of one carbon atom enables straightforward analysis of molecular structural changes by NMR. The HRMS spectrum revealed an anion signal of leuco-BODIPY with a mass-to-charge ratio (m/z) of 640.2280; this signal was ascribed to $[\text{BODIPY-OCH}_3]^-$ (Figure S4), indicating the formation of leuco-BODIPY. We assigned the proton signals of both forms of the dye by correlation spectroscopy (COSY) based on the ^{1}H−^{13}C NMR spectra. Based on the ^{1}H NMR spectra, addition of methanol to BODIPY in $CDCl_3$ caused the β-pyrrole proton closest to the meso-carbon to shift significantly upfield from 6.82 to 6.00 ppm (Figures S5, S9, and S13). This result suggests that the π-system of the indacene core became less extended upon formation of a tetrahedral geometry at the sp^3 meso-carbon of leuco-BODIPY. The ^{1}H NMR spectrum of leuco-BODIPY also reveals a similar upfield shift of the protons from the meso-pyridine group and the emergence of a new $-OCH_3$ peak at 3.79 ppm that proves the formation of leuco-BODIPY.[23] The ^{13}C NMR spectrum of leuco-BODIPY shows a new peak at 76.14 ppm (assigned to the sp^3 meso-carbon) and disappearance of the peak at 141.77 ppm (assigned to the sp^2 meso-carbon), amounting to an upfield shift of ~65.63 ppm. A new peak at 51.49 ppm can be assigned to the $-OCH_3$ group of leuco-BODIPY (Figures S6, S10, and S14). Lastly, we verified the recovery of BODIPY by adding acetic acid to leuco-BODIPY. We observed the reversion of the proton and carbon peaks of leuco-BODIPY to BODIPY and disappearance of the $-OCH_3$ peak at 3.79 ppm in the ^{1}H NMR spectrum and at 51.49 and 76.14 ppm in the ^{13}C NMR spectrum (Figures S11−S14), matching our previous results.[23]

We investigated the spectroscopic properties of the fluorescent probe as a function of pH in phosphate-buffered saline (PBS) containing 50% ethanol by UV−vis spectrophotometry and fluorimetry (Figures S15−S17). Adding 50% ethanol to PBS reflects the compromise between the need for solubilizing BODIPY in an aqueous environment and the need for proper reference to the conventional pH scale.[28,29] Under acidic conditions (pH ~ 4), the longest wavelength absorption band of BODIPY at 602 nm can be ascribed to the S0−S1 transition and the shoulder at 559 nm indicates the 0−1 vibrational band.[23,30] When compared to classical tetramethyl BODIPY dyes,[31] the absorption band of BODIPY is red-shifted from 500 to 602 nm, consistent with the extended π-system originating from the electron-withdrawing diethyl malonate groups coupling through their exocyclic double bonds at the 3,5-positions of the indacene core. The red emission peak of BODIPY appears at 618 nm. Conversely, after adding NaOH to adjust the medium to weakly basic conditions (pH ~ 7.4; indicative of the typical pH of culture medium), we observed that the main absorption band of BODIPY at 602 nm disappears and a new band of leuco-BODIPY appears near 360 nm. These absorption spectral changes were accompanied by a visible color change from magenta to light yellow and near-complete quenching of the red fluorescence. Reacidification of leuco-BODIPY by adding HCl led to the recovery of BODIPY,

https://doi.org/10.1021/acs.nanolett.1c03110
Nano Lett. 2021, 21, 9224−9232

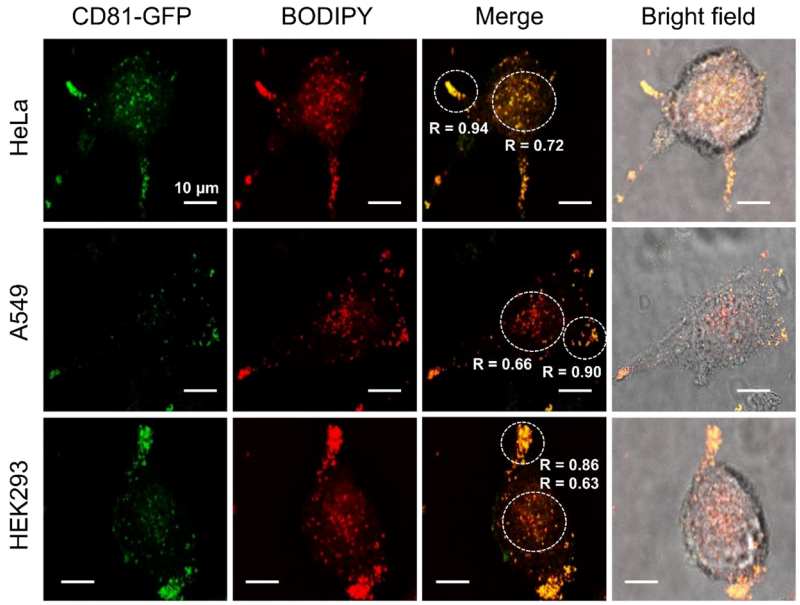

Figure 3. Detection of intracellular precursor EVs by this probe. HeLa cells, A549 cells, and HEK293 cells that express GFP-tagged CD81 (green) were added with leuco-BODIPY for 30 min and then imaged by confocal microscopy. Yellow color inside the cell indicates overlap of fluorescence between GFP-tagged CD81 (green) and BODIPY (red), with the strongest overlap located at the cell tips. *R* values indicate the Pearson colocalization coefficients between BODIPY and CD81-GFP. Scale bar = 10 μm.

as evidenced by the reappearance of the absorption bands at 602 nm with a pK_a of 5.28 ± 0.05 (corrected pK_a[32]) and the fluorescence bands at 618 nm. Closer inspection of the emission spectrum as a function of pH reflects the onset of the fluorescence peak at 618 nm at pH ∼ 7.4. As the pH drops from 7.4 to 7.0, 6.5, and further to 5.5, we observed a drastic ∼3-fold, 8-fold, and ∼15-fold increase in emission at 618 nm, respectively. The fluorescence intensity no longer increases with acidification when the pH falls below 5.25, due to the protonation of the nitrogen atom in the pyridine group of BODIPY.[33] We assessed the pH-reversible spectroscopic properties of the probe by monitoring the changes in absorbance at 602 nm (Figure S15E) upon switching the pH of the 1:1 (v/v) PBS/ethanol solution between 4.0 and 7.4 over three cycles. With an efficiency of recovery at 100% (within uncertainty), these reversible color changes between magenta at pH 4.0 and light yellow at pH 7.4 were confirmed by photography (Movie S1). Conversion from leuco-BODIPY to BODIPY is rapid, with a response half-life of absorbance recovery at 602 nm of 9 s (Figure S15F). To demonstrate the applicability of our probe under aqueous conditions, we further repeated the pH titration studies in water containing 0.5% (v/v) dimethyl sulfoxide (DMSO; for solubilizing the probe in culture medium for our later cell-based studies) and observed pH-responsive absorbance and fluorescence trends that are similar to those in 50% ethanol and 50% PBS (Figures S18−S21).

Before our cellular studies, we verified that incubation of HeLa, A549, and HEK293 cells with medium containing 2 μM leuco-BODIPY and 0.1% DMSO for 12 h did not severely reduce cell viability (Figure S22). We studied the mechanism for the cellular uptake of our probe by a pharmacological approach. Pretreatment of the three cell lines with sodium azide or preincubation of the cells at 4 °C[34] did not significantly affect the cellular uptake of our probe (Figure S23). These data indicate that energy-dependent endocytosis does not play a major role in cellular uptake; rather, the probe primarily enters the cell by diffusion, a result consistent with past reports on the cellular entry of other small molecular fluorescent probes.[35]

Then, we seeded HeLa, A549, or HEK293 cells that express GFP-tagged CD81 in a confocal dish and incubated the cells with phenol red-free medium containing 2 μM leuco-BODIPY and 0.1% DMSO for 30 min. Note that this probe is predominantly in its leuco-BODIPY form when dissolved in DMSO, as evidenced by its light-yellow color. We obtained confocal images of the cell-seeded medium without harvesting the EVs or rinsing the cells (Figure 2A and Figures S24 and S25). Representative images of their extracellular space depict granular or spherical pockets of fluorescence from BODIPY (red) amidst a dark background. Notably, such pockets of BODIPY fluorescence strongly colocalize with those of CD81-enriched exosomes (green), as evidenced by Pearson's colocalization coefficients of 0.92, 0.85, and 0.94 for HeLa, A549, and HEK293 cells, respectively. These data suggest the detection of exosomes with this probe. The fluorescent pockets of BODIPY are submicron-sized or micron-sized, larger than the reported sizes of exosomes (50−200 nm).[36] As the resolution limit of confocal microscopy may overestimate the size of EVs, we isolated EVs from the cell-seeded medium for nanoparticle tracking analysis (NTA; Figure 2B). The hydrodynamic size distribution of the EVs lies between ∼50 and ∼400 nm, with peak EV diameters of 151, 104, and 156 nm for HeLa, A549, and HEK293 cells, respectively. As these peak EV sizes corroborate the typical sizes of exosomes, we conclude that the EVs detected are mostly exosomes, with a smaller portion of larger ectosomes, clustered exosomes, or extracellular MVBs (to be discussed in Figure 4).

Moreover, we incubated the three cell types with our probe for 30 min, isolated the EVs secreted to the culture medium, centrifuged the collected medium to remove any dye-stained cell fragments, and confirmed the detection of fluorescence in the isolated EVs (Figure S26). By contrast, for the EVs isolated from the same cell types under the same culture conditions but

https://doi.org/10.1021/acs.nanolett.1c03110
Nano Lett. 2021, 21, 9224−9232

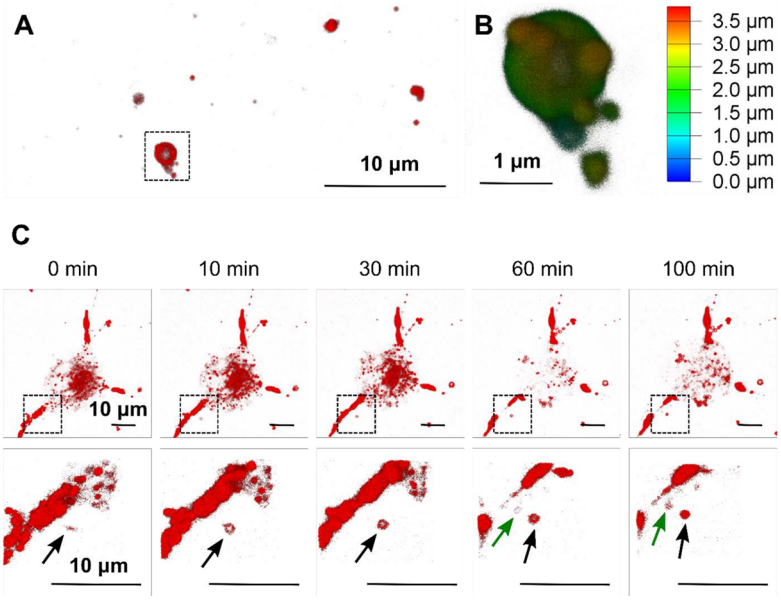

Figure 4. Visualizing extracellular multivesicular bodies (EMVBs) in the medium. (A) Confocal fluorescence images of HeLa cells were treated with leuco-BODIPY for 30 min and imaged by confocal microscopy. The serial focal planes were 0.3 μm apart and were illuminated. Red indicates the fluorescence of BODIPY. The 3D reconstruction images were generated by the Leica LAS-X software. Scale bar = 10 μm. (B) Enlarged images of the boxed area in panel A indicate EMVB-like large EVs. This image was generated with depth coding, using different colors to indicate the position of the *z*-axis. Scale bar = 1 μm. (C) Real-time formation of EMVBs as detected by this probe. HeLa cells were treated with leuco-BODIPY and imaged by confocal microscopy to generate time-series images. A series of focal plane images of 0.3 μm apart were recorded. Reconstructed 3D images were generated by the Leica LAS-X software. The bottom row shows the enlarged image of the boxed area in the top row. Arrows indicate real-time accumulation of EMVBs. Arrows in different colors (black and green) denote EMVBs at distinct extracellular locations. Scale bar = 10 μm.

without treatment by our probe, the fluorescence detected was at the background level of blank culture medium. As our probe does not fluoresce in the medium, the data suggest its localization in the EVs. Furthermore, previous studies showed that dyes used for labeling cells may affect cellular response.[37] Here, we isolated EVs from HeLa cells treated with our dye and those from unstained cells. NTA reveals that the size distributions of the EVs isolated from the dye-stained and unstained cells are similar (Figure S27), implying a limited effect of our probe on EV secretion.

To confirm that our observed BODIPY fluorescence does not stem from false positive artifacts, we took confocal images of a solution of leuco-BODIPY dissolved in medium at the same concentration (2 μM) but without cells seeded in the confocal dish. By using the same laser settings as our experimental group with cells seeded, we captured no detectable fluorescence 3 h post-incubation (Figure S28A) and limited signals 15 h post-incubation (Figure S28B). As a negative control, when we imaged phenol red-free medium containing LysoTracker Red (a commercial dye with a similar emission wavelength as BODIPY for staining acidic organelles) without cells seeded in the confocal dish, we detected false positive dot-like or speck-like signals when the dye concentration was 50 nM (as recommended by the manufacturer; Figure S28C) and severe background emission when the concentration was 2 μM (on par with our probe; Figure S28D) 3 h post-incubation. LysoTracker Red is a pH-insensitive dye with near-constant absorbance (Figures S29 and S30) and "always-on" fluorescence (Figures S31 and S32) across a pH range of 3−11. As LysoTracker Red may yield false positive signals if aggregated in medium, we did not use LysoTracker Red for further EV imaging studies. Collectively, the results underscore the importance of imaging EVs in medium by using dyes with limited (ideally zero) background to eliminate false positive signals that may bias image interpretation.

Next, we attempted to use our probe for imaging intracellular precursor EVs before their secretion to the extracellular milieu. Again, we added leuco-BODIPY (dissolved in DMSO) to culture medium seeded with HeLa, A549, or HEK293 cells that express GFP-tagged CD81 for 30 min (Figure 3). Representative confocal images of all cell types capture more intense pockets of BODIPY fluorescence (red) and GFP-CD81 fluorescence (green) on the pseudopodia (i.e., finger-like protrusions consisting of actin and microtubules[38,39]) of cell membrane than the cytoplasm, consistent with the role of CD81 in forming membrane protrusions,[40] regulating cell migration,[41] and secretion.[42] Notably, the imaging data depict strong overlap between BODIPY and GFP-CD81 fluorescence (yellow) on the pseudopodia, with Pearson's colocalization coefficients of 0.94, 0.90, and 0.86 for HeLa, A549, and HEK293 cells, respectively. Contrarily, the overlap between BODIPY and GFP-CD81 fluorescence in the cytoplasm is moderate, characterized by Pearson's colocalization coefficients of 0.72, 0.66, and 0.63 for HeLa, A549, and HEK293 cells, respectively. As a negative control, we captured confocal images of the three cell lines but without adding leuco-BODIPY to the medium. By using the same laser settings as our experimental group with leuco-BODIPY added, we did not detect appreciable levels of autofluorescence from the cells (Figure S33), confirming that our captured fluorescence signals originate from BODIPY. These data are consistent with the literature precedent that documented the localization of precursor EVs (e.g., MVBs) on the pseudopodia for secreting exosomes.[43]

https://doi.org/10.1021/acs.nanolett.1c03110
Nano Lett. 2021, 21, 9224−9232

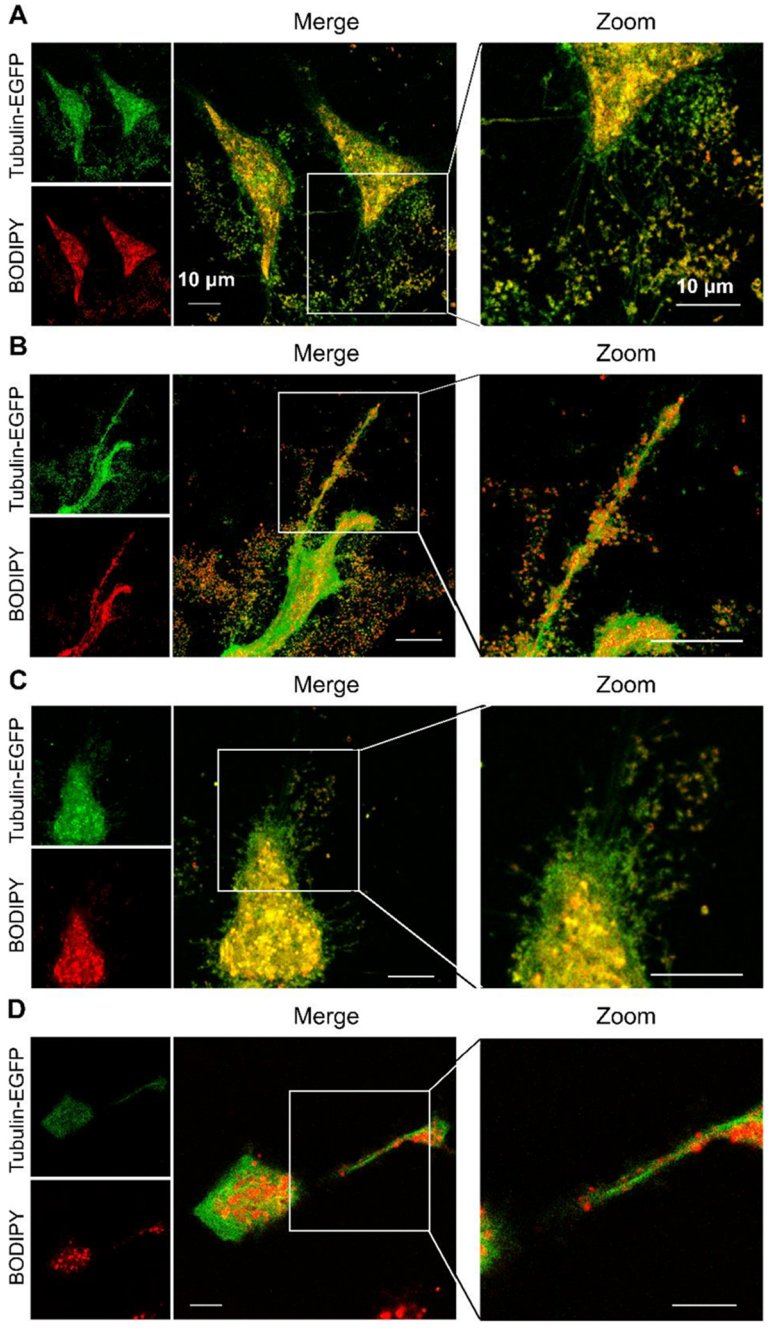

Figure 5. Transport of EVs along microtubules inside pseudopodia. (A, B) HeLa cells and (C, D) A549 cells were previously transfected with plasmid encoding EGFP-tagged tubulin before they were treated with leuco-BODIPY for 30 min and imaged by confocal microscopy. Red and green indicate BODIPY and EGFP fluorescence, respectively. Panels A and C show the thinner tubule fibers extended from the cell, and panels B and D show the thicker pseudopodia. The zoom column panels show the enlargement of the boxed area in the merge column panels. Scale bar = 10 μm.

We applied our probe to visualize the secretion of larger types of EVs than exosomes, because our NTA data indicate an EV size range of 50−900 nm (Figure 2B). After adding leuco-BODIPY to medium seeded with HeLa cells, we observed by confocal imaging EMVBs that measure ∼1 μm in diameter and resemble MVBs rather than clusters of exosomes in the medium (Figure 4A). Our three-dimensionally reconstructed image of a representative EMVB portrays smaller exosomes inside or near an MVB-like microvesicle (Figure 4B). To gain insights into EV secretion, we added leuco-BODIPY to HeLa cells and captured a representative extracellular area adjacent to the pseudopodium of a cell (Figure 4C and Movie S2). Time-course confocal imaging for ∼100 min reveals the formation of donut-shaped microvesicles near the pseudopodium (green and black arrows), matching our observation of the overlapping fluorescence between CD81 and BODIPY (Figure 3). These data led us to hypothesize the involvement of pseudopodia in EV secretion because previous reports documented a linkage between exocytic events and pseudopodia formation.[42]

Passive diffusion is an established mode of transport for EVs to reach an extracellular region distant from the originating

https://doi.org/10.1021/acs.nanolett.1c03110
Nano Lett. 2021, 21, 9224−9232

cell,[44,45] yet our mechanistic understanding in the active transport of precursor EVs to the extracellular milieu remains limited. Classically, cytoskeleton elements such as actin[46] and microtubule[47] regulate the formation and movement of pseudopodia; whereas the formation of lamellipodia occurs *via* actin polymerization independently of microtubules, microtubules are required for cell migration, tail retraction, and modulation of cell adhesion.[48] A recent study reveals that, in migrating cells, intraluminal vesicle (ILV)-containing microvesicles grow on degenerative, branched thin pseudopodia (i.e., retraction fibers) that eventually degenerate and release the ILVs in the extracellular space as EVs.[49] As retraction fibers are rich in actin,[50] this study suggests the involvement of actin filaments in EV secretion. Here, we questioned if microtubules participate in the extracellular transport of EVs because, like actin filaments, microtubules also serve as intracellular trackways for transporting vesicles. To this end, we applied our probe in combination with plasmid transfection to visualize the transport of EVs along microtubules inside pseudopodia. After transfecting HeLa and A549 cells with plasmids that encode tubulin-6 (a major constituent of microtubules) tagged with enhanced green fluorescent protein (EGFP) for 1−3 d, we incubated the cells with leuco-BODIPY for 30 min (Figure 5). Confocal imaging depicts the distribution of tubulin-6 in thinner strands that resemble retraction fibers[49] (Figure 5A,C) and thicker pseudopodia that are branched and shaped like leaf veins (Figure 5B,D). For both cell types tested, we detected the alignment of precursor EVs to the thinner strands and along the thicker pseudopodia. Time-lapse imaging confirms the movement of EVs along the microtubules away from the cell (Movies S3 and S4) These data demonstrate the utility of our probe for visualizing the transport of precursor EVs before their release as EVs.

In conclusion, our pH-reversible molecular fluorescent probe supports *in situ* visualization of EVs (say CD81-enriched exosomes) in three cell types and the secretion of EVs from living cells without inducing severe cytotoxicity. Careful design of the BODIPY core-reactive molecular structure enables the adjustment of its pK_a, onset point of fluorescence, and pH-dependent photophysical properties for visualizing cellular processes. Upon attack by nucleophiles, the probe switches from its parent BODIPY form that emits bright magenta fluorescence to its non-fluorescent leuco-BODIPY form. Conversely, after engaging secreted EVs in the medium or intracellular precursor EVs containing acidic lumen, leuco-BODIPY reverts to BODIPY with an onset point of fluorescence at pH ∼ 7.4. This probe not only obviates the need for EV isolation prior to imaging but also supports imaging of EVs in medium with pronouncedly attenuated false positive signals when compared to "always-on" fluorescent dyes. Finally, our probe may offer insights into the mechanism for EV secretion. By applying our probe jointly with plasmid transfection, we have proven that some precursor EVs traverse along microtubules in the pseudopodia before their secretion as EVs. This result enhances our knowledge in the interplay between the cytoskeleton network and EV secretion. Currently, this probe alone does not enable specific delineation between different types of intracellular organelles (MVBs versus lysosomes) or different types of EVs (exosomes versus EMVBs), because our detection mechanism is primarily based on pH. Still, one may derive insights into the origin of EVs by combining this probe with transfection of plasmids encoding different markers of precursor EVs (e.g., Rab9 for late endosomes and LAMP-1 for lysosomes[51]). Keeping in mind the simple staining procedure of our probe and the flexibility of transfecting plasmids encoding different genes of interest, we anticipate that our probe will empower researchers to interrogate other biological pathways of EV secretion, spurring the development of EV-based nanomedicines. Lastly, because fluorescent probes that can reveal physiological processes[52] and disease states[53] in preclinical models are on the horizon, we envision the future development of probes for imaging EVs *in vivo*.

■ ASSOCIATED CONTENT

Supporting Information

The Supporting Information is available free of charge at https://pubs.acs.org/doi/10.1021/acs.nanolett.1c03110.

Synthesis scheme of BODIPY, IUPAC naming of the atoms of the BODIPY structure, absorption and fluorescence spectra of BODIPY and leuco-BODIPY, HRMS spectra of BODIPY and leuco-BODIPY, ^{1}H and ^{13}C NMR spectra of BODIPY and leuco-BODIPY, cytotoxicity of the probe, pathway for the cellular uptake of the probe, fluorescence signal of the probe per EV, effect of probe staining on the hydrodynamic size distribution of EVs, and additional confocal images (PDF)

Movie S1: Color-changing reversible cycles of the probe (AVI)

Movie S2: Real-time secretion of EMVBs (AVI)

Movie S3: Time-lapse imaging of the release of EVs along microtubes (AVI)

Movie S4: Enlarged time-lapse imaging of the release of EVs along microtubes (AVI)

■ AUTHOR INFORMATION

Corresponding Author

Chung Hang Jonathan Choi − *Department of Biomedical Engineering, The Chinese University of Hong Kong, Shatin, New Territories, Hong Kong SAR;* orcid.org/0000-0003-2935-7217; Email: jchchoi@cuhk.edu.hk

Authors

Hanzhuang Liu − *Department of Biomedical Engineering, The Chinese University of Hong Kong, Shatin, New Territories, Hong Kong SAR;* orcid.org/0000-0003-3860-6967

Shaorui Liu − *Department of Surgery, The Chinese University of Hong Kong, Shatin, New Territories, Hong Kong SAR;* orcid.org/0000-0003-2408-9137

Yu Xiao − *Department of Biomedical Engineering, The Chinese University of Hong Kong, Shatin, New Territories, Hong Kong SAR*

Wenting Song − *State Key Laboratory of Coordination Chemistry, School of Chemistry and Chemical Engineering, Nanjing University, Nanjing 210023, China*

Huize Li − *Department of Biomedical Engineering, The Chinese University of Hong Kong, Shatin, New Territories, Hong Kong SAR*

Lok Wai Cola Ho − *Department of Biomedical Engineering, The Chinese University of Hong Kong, Shatin, New Territories, Hong Kong SAR;* orcid.org/0000-0003-3260-9032

Zhen Shen − *State Key Laboratory of Coordination Chemistry, School of Chemistry and Chemical Engineering,*

Nanjing University, Nanjing 210023, China; orcid.org/0000-0003-2464-1278

Complete contact information is available at: https://pubs.acs.org/10.1021/acs.nanolett.1c03110

Notes

The authors declare no competing financial interest.

■ ACKNOWLEDGMENTS

This work was in part supported by the Chow Yuk Ho Technology Centre for Innovative Medicine and a Vice-Chancellor Discretionary Fund from The Chinese University of Hong Kong (CUHK). C.H.J.C. acknowledges a Croucher Innovation Award from the Croucher Foundation. We thank Ruifang Han, Yee Ting Elaine Chiu, Cecilia Ka Wing Chan, and Yao Liu from the Department of Biomedical Engineering at CUHK for helpful discussions. We thank Chun Wah Lin from the Department of Chemistry at CUHK for support in fluorimetry and Katie Meehan from the Department of Otorhinolaryngology at CUHK for advice on NTA.

■ REFERENCES

(1) Kalluri, R.; LeBleu, V. S. The Biology, Function, and Biomedical Applications of Exosomes. *Science* **2020**, *367* (6478), No. eaau6977.

(2) Shao, H.; Im, H.; Castro, C. M.; Breakefield, X.; Weissleder, R.; Lee, H. New Technologies for Analysis of Extracellular Vesicles. *Chem. Rev.* **2018**, *118* (4), 1917−1950.

(3) Al-Nedawi, K.; Meehan, B.; Micallef, J.; Lhotak, V.; May, L.; Guha, A.; Rak, J. Intercellular Transfer of the Oncogenic Receptor EGFRvIII by Microvesicles Derived from Tumour Cells. *Nat. Cell Biol.* **2008**, *10* (5), 619−624.

(4) Fais, S.; O'Driscoll, L.; Borras, F. E.; Buzas, E.; Camussi, G.; Cappello, F.; Carvalho, J.; Cordeiro da Silva, A.; Del Portillo, H.; El Andaloussi, S.; Ficko Trček, T.; Furlan, R.; Hendrix, A.; Gursel, I.; Kralj-Iglic, V.; Kaeffer, B.; Kosanovic, M.; Lekka, M. E.; Lipps, G.; Logozzi, M.; Marcilla, A.; Sammar, M.; Llorente, A.; Nazarenko, I.; Oliveira, C.; Pocsfalvi, G.; Rajendran, L.; Raposo, G.; Rohde, E.; Siljander, P.; van Niel, G.; Vasconcelos, M. H.; Yáñez-Mó, M.; Yliperttula, M. L.; Zarovni, N.; Zavec, A. B.; Giebel, B. Evidence-Based Clinical Use of Nanoscale Extracellular Vesicles in Nanomedicine. *ACS Nano* **2016**, *10* (4), 3886−3899.

(5) Yong, T.; Zhang, X.; Bie, N.; Zhang, H.; Zhang, X.; Li, F.; Hakeem, A.; Hu, J.; Gan, L.; Santos, H. A.; Yang, X. Tumor Exosome-Based Nanoparticles are Efficient Drug Carriers for Chemotherapy. *Nat. Commun.* **2019**, *10* (1), 3838.

(6) Meldolesi, J. Exosomes and Ectosomes in Intercellular Communication. *Curr. Biol.* **2018**, *28* (8), R435−R444.

(7) Cocucci, E.; Meldolesi, J. Ectosomes and Exosomes: Shedding the Confusion Between Extracellular Vesicles. *Trends Cell Biol.* **2015**, *25* (6), 364−372.

(8) Shen, L.-M.; Quan, L.; Liu, J. Tracking Exosomes *in Vitro* and *in Vivo* To Elucidate Their Physiological Functions: Implications for Diagnostic and Therapeutic Nanocarriers. *ACS Appl. Nano Mater.* **2018**, *1* (6), 2438−2448.

(9) Miesenböck, G.; De Angelis, D. A.; Rothman, J. E. Visualizing Secretion and Synaptic Transmission with pH-sensitive Green Fluorescent Proteins. *Nature* **1998**, *394* (6689), 192−195.

(10) Sung, B. H.; von Lersner, A.; Guerrero, J.; Krystofiak, E. S.; Inman, D.; Pelletier, R.; Zijlstra, A.; Ponik, S. M.; Weaver, A. M. A Live Cell Reporter of Exosome Secretion and Uptake Reveals Pathfinding Behavior of Migrating Cells. *Nat. Commun.* **2020**, *11* (1), 2092.

(11) Ma, B.; Zhang, S.; Jiang, H.; Zhao, B.; Lv, H. Lipoplex Morphologies and Their Influences on Transfection Efficiency in Gene Delivery. *J. Controlled Release* **2007**, *123* (3), 184−194.

(12) Dass, C. R. Lipoplex-mediated Delivery of Nucleic Acids: Factors Affecting *in vivo* Transfection. *J. Mol. Med.* **2004**, *82* (9), 579−591.

(13) Feng, L.; Xie, Y.; Au-Yeung, S. K.; Hailu, H. B.; Liu, Z.; Chen, Q.; Zhang, J.; Pang, Q.; Yao, X.; Yang, M.; Zhang, L.; Sun, H. A Fluorescent Molecular Rotor Probe for Tracking Plasma Membranes and Exosomes in Living Cells. *Chem. Commun.* **2020**, *56* (60), 8480−8483.

(14) Zhou, X.; Zhang, J.; Song, Z.; Lu, S.; Yu, Y.; Tian, J.; Li, X.; Guan, F. ExoTracker: A Low-pH-Activatable Fluorescent probe for Labeling Exosomes and Monitoring Endocytosis and Trafficking. *Chem. Commun.* **2020**, *56* (94), 14869−14872.

(15) Lyu, Y.; Cui, D.; Huang, J.; Fan, W.; Miao, Y.; Pu, K. Near-Infrared Afterglow Semiconducting Nano-Polycomplexes for the Multiplex Differentiation of Cancer Exosomes. *Angew. Chem., Int. Ed.* **2019**, *58* (15), 4983−4987.

(16) Wang, L.; Hiblot, J.; Popp, C.; Xue, L.; Johnsson, K. Environmentally Sensitive Color-Shifting Fluorophores for Bioimaging. *Angew. Chem., Int. Ed.* **2020**, *59* (49), 21880−21884.

(17) Chan, J.; Dodani, S. C.; Chang, C. J. Reaction-Based Small-Molecule Fluorescent Probes for Chemoselective Bioimaging. *Nat. Chem.* **2012**, *4*, 973−984.

(18) Kashima, H.; Kamiya, M.; Obata, F.; Kojima, R.; Nakano, S.; Miura, M.; Urano, Y. Photoactivatable Fluorophores for Durable Labelling of Individual Cells. *Chem. Commun.* **2021**, *57*, 5802−5805.

(19) Iwaki, H.; Kamiya, M.; Kawatani, M.; Kojima, R.; Yamasoba, T.; Urano, Y. Fluorescence Probes for Imaging Basic Carboxypeptidase Activity in Living Cells with High Intracellular Retention. *Anal. Chem.* **2021**, *93* (7), 3470−3476.

(20) Obara, R.; Kamiya, M.; Tanaka, Y.; Abe, A.; Kojima, R.; Kawaguchi, T.; Sugawara, M.; Takahashi, A.; Noda, T.; Urano, Y. γ-Glutamyltranspeptidase (GGT)-Activatable Fluorescence Probe for Durable Tumor Imaging. *Angew. Chem., Int. Ed.* **2021**, *60* (4), 2125−2129.

(21) Hu, D.; Zhang, T.; Li, S.; Yu, T.; Zhang, X.; Hu, R.; Feng, J.; Wang, S.; Liang, T.; Chen, J.; Sobenina, L. N.; Trofimov, B. A.; Li, Y.; Ma, J.; Yang, G. Ultrasensitive Reversible Chromophore Reaction of BODIPY Functions as High Ratio Double Turn on probe. *Nat. Commun.* **2018**, *9* (1), 362.

(22) Ma, L.; Ouyang, Q.; Werthmann, G. C.; Thompson, H. M.; Morrow, E. M. Live-Cell Microscopy and Fluorescence-Based Measurement of Luminal pH in Intracellular Organelles. *Front. Cell Dev. Biol.* **2017**, *5*, 71.

(23) Liu, H.; Song, W.; Gröninger, D.; Zhang, L.; Lu, Y.; Chan, K. S.; Zhou, Z.; Rurack, K.; Shen, Z. Real-time Monitoring of Newly Acidified Organelles During Autophagy Enabled by Reaction-Based BODIPY Dyes. *Commun. Biol.* **2019**, *2* (1), 442.

(24) Teknikel, E.; Unaleroglu, C. Colorimetric and fluorometric pH sensor based on bis(methoxycarbonyl)ethenyl functionalized BODIPY. *Dyes Pigm.* **2015**, *120*, 239−244.

(25) Wallace, P. K.; Tario, J. D., Jr.; Fisher, J. L.; Wallace, S. S.; Ernstoff, M. S.; Muirhead, K. A. Tracking Antigen-Driven Responses by Flow Cytometry: Monitoring Proliferation by Dye Dilution. *Cytometry, Part A* **2008**, *73A* (11), 1019−1034.

(26) Chuo, S. T.-Y.; Chien, J. C.-Y.; Lai, C. P.-K. Imaging Extracellular Vesicles: Current and Emerging Methods. *J. Biomed. Sci.* **2018**, *25* (1), 91.

(27) Loudet, A.; Burgess, K. BODIPY Dyes and Their Derivatives: Syntheses and Spectroscopic Properties. *Chem. Rev.* **2007**, *107* (11), 4891−4932.

(28) Liu, H.; Song, W.; Zhang, S.; Chan, K. S.; Guo, Z.; Shen, Z. A Ratiometric Fluorescent Probe for Real-Time Monitoring of Intracellular Glutathione Fluctuations in Response to Cisplatin. *Chem. Sci.* **2020**, *11* (32), 8495−8501.

(29) Wang, Y.-W.; Descalzo, A. B.; Shen, Z.; You, X.-Z.; Rurack, K. Dihydronaphthalene-Fused Boron-Dipyrromethene (BODIPY) Dyes: Insight into the Electronic and Conformational Tuning Modes of BODIPY Fluorophores. *Chem. - Eur. J.* **2010**, *16* (9), 2887−2903.

(30) Kollmannsberger, M.; Rurack, K.; Resch-Genger, U.; Daub, J. Ultrafast Charge Transfer in Amino-Substituted Boron Dipyrromethene Dyes and Its Inhibition by Cation Complexation: A New Design Concept for Highly Sensitive Fluorescent Probes. *J. Phys. Chem. A* **1998**, *102* (50), 10211−10220.
(31) Lu, H.; Mack, J.; Yang, Y.; Shen, Z. Structural Modification Strategies for the Rational Design of Red/NIR region BODIPYs. *Chem. Soc. Rev.* **2014**, *43* (13), 4778−4823.
(32) Maus, M.; Rurack, K. Monitoring pH and Solvent Proticity with Donor-Acceptor-Substituted Biphenyls: A New Approach Towards Highly Sensitive and Powerful Fluorescent Probes by Tuning the Molecular Structure. *New J. Chem.* **2000**, *24* (9), 677−686.
(33) Krygowski, T. M.; Szatyłowicz, H.; Zachara, J. E. How H-Bonding Modifies Molecular Structure and π-Electron Delocalization in the Ring of Pyridine/Pyridinium Derivatives Involved in H-Bond Complexation. *J. Org. Chem.* **2005**, *70* (22), 8859−8865.
(34) Liu, Y.; Choi, C. K. K.; Hong, H.; Xiao, Y.; Kwok, M. L.; Liu, H.; Tian, X. Y.; Choi, C. H. J. Dopamine Receptor-Mediated Binding and Cellular Uptake of Polydopamine-Coated Nanoparticles. *ACS Nano* **2021**, *15* (8), 13871−13890.
(35) Xu, W.; Zeng, Z.; Jiang, J. H.; Chang, Y. T.; Yuan, L. Discerning the Chemistry in Individual Organelles with Small-Molecule Fluorescent Probes. *Angew. Chem., Int. Ed.* **2016**, *55* (44), 13658−13699.
(36) Kalishwaralal, K.; Kwon, W. Y.; Park, K. S. Exosomes for Non-Invasive Cancer Monitoring. *Biotechnol. J.* **2019**, *14* (1), 1800430.
(37) Homolya, L.; Holló, Z.; Germann, U. A.; Pastan, I.; Gottesman, M. M.; Sarkadi, B. Fluorescent Cellular Indicators are Extruded by the Multidrug Resistance Protein. *J. Biol. Chem.* **1993**, *268* (29), 21493−21496.
(38) Mikhailov, A.; Gundersen, G. G. Relationship Between Microtubule Dynamics and Lamellipodium Formation Revealed by Direct Imaging of Microtubules in Cells Treated with Nocodazole or Taxol. *Cell Motil. Cytoskeleton* **1998**, *41* (4), 325−340.
(39) Tang, D. D.; Gerlach, B. D. The Roles and Regulation of the Actin Cytoskeleton, Intermediate Filaments and Microtubules in Smooth Muscle Cell Migration. *Respir. Res.* **2017**, *18* (1), 54.
(40) Quast, T.; Eppler, F.; Semmling, V.; Schild, C.; Homsi, Y.; Levy, S.; Lang, T.; Kurts, C.; Kolanus, W. CD81 is Essential for the Formation of Membrane Protrusions and Regulates Rac1-Activation in Adhesion-Dependent Immune Cell Migration. *Blood* **2011**, *118* (7), 1818−1827.
(41) Chambrion, C.; Le Naour, F. The Tetraspanins CD9 and CD81 Regulate CD9P1-Induced Effects on Cell Migration. *PLoS One* **2010**, *5* (6), No. e11219.
(42) Sesaki, H.; Ogihara, S. Protrusion of Cell Surface Coupled with Single Exocytotic Events of Secretion of the Slime in Physarum Plasmodia. *J. Cell Sci.* **1997**, *110* (7), 809−818.
(43) Hoshino, D.; Kirkbride, K. C.; Costello, K.; Clark, E. S.; Sinha, S.; Grega, L. N.; Tyska, M. J.; Weaver, A. M. Exosome Secretion is Enhanced by Invadopodia and Drives Invasive Behavior. *Cell Rep.* **2013**, *5* (5), 1159−1168.
(44) Kastelowitz, N.; Yin, H. Exosomes and Microvesicles: Identification and Targeting by Particle Size and Lipid Chemical Probes. *ChemBioChem* **2014**, *15* (7), 923−928.
(45) McKelvey, K. J.; Powell, K. L.; Ashton, A. W.; Morris, J. M.; McCracken, S. A. Exosomes: Mechanisms of Uptake. *J. Circ. Biomark.* **2015**, *4*, 7.
(46) Lee, E.; Shelden, E. A.; Knecht, D. A. Changes in Actin Filament Organization during Pseudopod Formation. *Exp. Cell Res.* **1997**, *235* (1), 295−299.
(47) Ueda, M.; Ogihara, S. Microtubules are Required in Amoeba Chemotaxis for Preferential Stabilization of Appropriate Pseudopods. *J. Cell Sci.* **1994**, *107* (8), 2071−2079.
(48) Ballestrem, C.; Wehrle-Haller, B.; Hinz, B.; Imhof, B. A. Actin-Dependent Lamellipodia Formation and Microtubule-Dependent Tail Retraction Control-Directed Cell Migration. *Mol. Biol. Cell* **2000**, *11* (9), 2999−3012.
(49) Ma, L.; Li, Y.; Peng, J.; Wu, D.; Zhao, X.; Cui, Y.; Chen, L.; Yan, X.; Du, Y.; Yu, L. Discovery of the Migrasome, An Organelle Mediating Release of Cytoplasmic Contents during Cell Migration. *Cell Res.* **2015**, *25* (1), 24−38.
(50) Cramer, L. P.; Mitchison, T. J. Investigation of the Mechanism of Retraction of the Cell Margin and Rearward Flow of Nodules during Mitotic Cell Rounding. *Mol. Biol. Cell* **1997**, *8* (1), 109−119.
(51) Ho, L. W. C.; Yung, W.-Y.; Sy, K. H. S.; Li, H. Y.; Choi, C. K. K.; Leung, K. C.-F.; Lee, T. W. Y.; Choi, C. H. J. Effect of Alkylation on the Cellular Uptake of Polyethylene Glycol-Coated Gold Nanoparticles. *ACS Nano* **2017**, *11* (6), 6085−6101.
(52) Cheng, P.; Pu, K., Molecular Imaging and Disease Theranostics with Renal-Clearable Optical Agents. *Nat. Rev. Mater.* **2021**. DOI: 10.1038/s41578-021-00328-6.
(53) Huang, J.; Li, J.; Lyu, Y.; Miao, Q.; Pu, K. Molecular Optical Imaging Probes for Early Diagnosis of Drug-Induced Acute Kidney Injury. *Nat. Mater.* **2019**, *18* (10), 1133−1143.

https://doi.org/10.1021/acs.nanolett.1c03110
Nano Lett. 2021, 21, 9224−9232